Heat Capacity and Antiferromagnetic Phase Transition of the Organic Free Radical Magnet, 2-*tert*-Butylaminoxylbenzimidazole (BABI)†

Yuji Miyazaki,‡ Takeshi Sakakibara,‡ Jacqueline R. Ferrer,§ Paul M. Lahti,*,§ Guillermo Antorrena,|| Fernando Palacio,|| and Michio Sorai*,‡

Research Center for Molecular Thermodynamics, Graduate School of Science, Osaka University, Toyonaka, Osaka 560-0043, Japan, Department of Chemistry 701, University of Massachusetts, Amherst, Massachusetts 01003-9336, and Instituto de Ciencia de Materiales de Aragón, CSIC−Universidad de Zaragoza, 50009 Zaragoza, Spain

Received: March 6, 2002; In Final Form: May 24, 2002

Heat capacities of the organic free radical magnet 2-*tert*-butylaminoxylbenzimidazole (BABI) have been measured in the 0.2−300 K range by adiabatic calorimetry for investigation of its magnetic properties from a thermodynamic viewpoint. An antiferromagnetic phase transition was observed at $T_N = 1.7$ K. A heat capacity hump arising from short-range spin ordering characteristic of low-dimensional magnets was found around 2 K. The magnetic enthalpy and entropy were determined to be 17.4 J mol^{-1} and 5.34 J K^{-1} mol^{-1}, respectively. The magnitude of the magnetic entropy is in good agreement with the theoretical value for the magnetic ordering of spin quantum number $S = {}^1/_2$ systems, $R \ln 2 = 5.76$ J K^{-1} mol^{-1}, where R is the gas constant. The heat capacity hump above T_N is well reproduced by the $S = {}^1/_2$ two-dimensional antiferromagnetic bilayer Heisenberg model with the intralayer interaction $J_1/k_B = -1.2$ K and the interlayer interaction $J_2/k_B = -1.9$ K, where k_B is the Boltzmann constant. The bilayer model gives a close fit to both the present calorimetric and previously reported magnetic data with very similar intra- and interlayer exchange interaction parameters. Lower dimensionality models (such as dimeric interaction) for the magnetic and heat capacity behavior are not consistent with experimental results.

1. Introduction

Molecule-based magnets mainly consisting of organic constituents have widely been synthesized and extensively investigated because of their interesting magnetic properties which are different from usual inorganic magnets composed of metals or metal oxides. Particularly, pure organic magnets have attracted many organic and physical chemists, in efforts to design specific molecule-based structures. So far, many examples of organic free radical magnets have been prepared and investigated.[1−14]

One of promising strategies for controlling packing of organic free radicals in the solid state is to use hydrogen bonding. For instance, Sugawara et al.[8] and Veciana et al.[10] showed that hydrogen-bonding hydroxyphenyl and dihydroxyphenyl groups may be linked to stable nitronylnitroxide radicals to yield organic magnets with spin ordering. Yoshioka et al.[14] attached hydrogen-bonding imidazole and benzimidazole groups to nitronylnitroxide spin-bearing centers to make stable radical solids with spin ordering.

Recently, Ferrer et al.[15] synthesized a new organic free radical, 2-*tert*-butylaminoxylbenzimidazole (BABI for short), which is stable to air at room temperature. The molecular structure of BABI is drawn in Figure 1. The X-ray crystallographic analysis of BABI crystal at room temperature[15] revealed that BABI exhibits an orthorhombic crystal lattice with space group *Pbca*. In the lattice, BABI radicals stack along the *a* axis and are hydrogen-bonded through N−H···N interactions of the benzimidazole moiety along the *b* axis to produce pseudo-two-dimensional sheets. One sheet is related to the other sheet by a typical benzenoid herringbone arrangement to form a bilayer with its nitroxide groups arrayed on the outside and its benzimidazole aromatic cores on the inside. One bilayer is related to a neighboring bilayer by a center of symmetry, leading to a nearest O···O distance (4.86 Å) between the nitroxide groups.

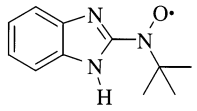

Figure 1. Molecular structure of BABI.

On the bases of magnetic susceptibility measurements of the polycrystalline BABI between 1.8 and 300 K, Ferrer et al.[15] found that the susceptibility follows a Curie−Weiss law over 10−300 K, with the spin quantum number $S = {}^1/_2$, the Weiss constant $\theta = -4.24(4)$ K, and the Landé g-factor $g = 2.029(3)$. They tried to fit various models to the experimental data and found that the best fit is an $S = {}^1/_2$ square-planar two-dimensional Heisenberg model with the exchange interaction $J/k_B = -1.60$ K when assuming $g = 2$, where k_B is Boltzmann's constant, and the spin Hamiltonian is assumed to be $H = -2JS_i \cdot S_j$. Although they did not observe the Néel magnetic phase transition temperature T_N at temperatures down to 1.8 K, their

† Contribution no. 62 from the Research Center for Molecular Thermodynamics.

* Authors for correspondence: Paul M. Lahti (Tel: +1-413-545-2318. Fax: +1-413-545-4490. E-mail: lahti@chem.umass.edu.) and Michio Sorai (Tel: +81-6-6850-5523. Fax: +81-6-6850-5526. E-mail: sorai@chem.sci.osaka-u.ac.jp.).

‡ Research Center for Molecular Thermodynamics.

§ Department of Chemistry.

|| Instituto de Ciencia de Materiales de Aragón.

10.1021/jp020630i CCC: $22.00
Published on Web 07/31/2002

data suggested that the transition would be just below the experimental minimum for their apparatus.

Adiabatic heat capacity calorimetry for magnetic substances is one of the most powerful methods for investigation of their magnetic properties, because one can gain the information about precise magnetic phase transition temperatures, degrees of spin ordering, spin−spin interaction, magnetic dimensionality, and type of magnetism. The Sorai group has extensively elucidated the magnetic properties of several organic free radical magnets by adiabatic heat capacity calorimetry.[4a,b,e,f,9h] In the present paper, we report the precise and accurate calorimetric studies of polycrystalline BABI to reveal further aspects of its magnetic properties, beyond those obtained by magnetic study.[15]

2. Experimental Section

BABI crystals were prepared according to the procedure described earlier.[15] The result of elemental analysis of the obtained crystal was as follows. Calcd for $C_{11}H_{14}N_3O$: C, 64.69; H, 6.91; N, 20.57. Found: C, 64.29; H, 6.88; N, 20.31.

Two apparatus were employed for the heat capacity measurement of the sample, to cover different temperature regions. Over the 0.2−28 K range, a very-low-temperature adiabatic calorimeter equipped with a ^{3}He/^{4}He dilution refrigerator[16] was used. A pressed disk of BABI (0.80183 g), 2 cm in diameter and ca. 2 mm in thickness, was put into a gold-plated copper sample holder without any heat exchange medium. Thermometry was done using a germanium resistance thermometer (Cryo Cal Inc., CR100) and a carbon resistor, the temperature scale of which is based on EPT-76. Over the 6−300 K region, a low-temperature adiabatic microcalorimeter[17] was utilized. A sample of 0.80854 g was loaded into a gold-plated copper vessel and sealed with 0.1 MPa of helium gas to aid thermal equilibration. A rhodium−iron resistor (Oxford Instruments Co., PHZ0012) was used for thermometry in the ITS-90 temperature scale. Buoyancy correction for the sample masses was made by use of the sample density $d = 1.223$ g cm^{-3}.[15]

In case of measurement with the lower temperature apparatus, the contribution of the sample to the whole heat capacity (sample + sample holder) was less than ca. 4% above 18 K, which caused disagreement with the heat capacity data by the latter calorimeter. On the other hand, the heat capacity data obtained using the higher temperature calorimeter deviated below 12 K from those obtained with the lower temperature calorimeter. This arises from an apparent increase due to desorption from the sample of the helium gas used as the heat exchange medium.

3. Results and Discussion

A. Heat Capacity. Molar heat capacities C_p of BABI crystal are tabulated in Table 1 and plotted against temperature T in Figure 2. A heat capacity cusp was observed at 1.7 K, which can be attributed to the antiferromagnetic phase transition. Above 1.7 K, a heat capacity hump centered around 2 K was also observed. This thermal anomaly may be ascribed to short-range order characteristic of low-dimensional magnets, consistent with the magnetic study[15] suggesting that BABI crystal belongs to a square-planar two-dimensional Heisenberg spin system.

In addition to these magnetic heat capacity anomalies, a sluggish thermal anomaly was found at around 200 K. This anomaly appears to be a glass transition, judging by its shape. The origin of this glass transition will be discussed later.

B. Determination of Lattice and Magnetic Heat Capacities. To separate the magnetic contribution from the total heat capacity data, it is necessary to determine the lattice heat capacity C_{lat}. At low temperatures, the following odd-power temperature-polynomial is often a good approximation:

$$C_{\mathrm{lat}} = \sum_{i=1}^{n} c_i T^{2i+1} \tag{1}$$

which corresponds to a series expansion of the Debye function with respect to T. Since magnetic heat capacities at high enough temperatures can be expressed by a term proportional to T^{-2},[18] the experimental heat capacities of magnetic materials—at temperatures high enough above magnetic thermal anomalies but low enough where the lattice heat capacities can be approximated by eq 1—are given by

$$C_p = \sum_{i=1}^{n} c_i T^{2i+1} + c_{n+1} T^{-2} \tag{2}$$

For the present BABI sample, we could fit eq 2 quite well to the heat capacity data from 4 to 10 K, when $n = 3$ with $c_1 = 3.282 \times 10^{-3}$ J K^{-4} mol^{-1}, $c_2 = -1.936 \times 10^{-5}$ J K^{-6} mol^{-1}, $c_3 = 1.397 \times 10^{-7}$ J K^{-8} mol^{-1}, and $c_4 = 31.33$ J K mol^{-1}. The estimated lattice heat capacity curve is shown in Figure 2a by a solid curve.

The magnetic heat capacity ΔC_p was derived by subtraction of the lattice heat capacity (eq 1) from the total heat capacity. Parts a and b of Figure 3 show a plot of ΔC_p versus T in both logarithmic and normal scales. Enhanced views are given in Figure 3 of a heat capacity cusp of an antiferromagnetic phase transition at $T_N = 1.7$ K, and a heat capacity hump due to short-range ordering of the spin system around 2 K.

C. Magnetic Enthalpy and Entropy Gains Due to Magnetic Origin. The enthalpy and entropy gains due to the magnetic effects in BABI were evaluated as follows. The enthalpy and entropy changes due to magnetic effects below the lowest measurement temperature of 0.2 K were estimated on the basis of the spin wave theory that will be given in more detail later. Those between 0.2 and 10 K were calculated by direct integration of the ΔC_p values with respect to T and ln T, respectively. Evaluation of those from 10 K to infinite temperature was done by use of the T^{-2} term of eq 2. The magnetic enthalpy and entropy changes thus evaluated were 17.4 J mol^{-1} and 5.34 J K^{-1} mol^{-1}, respectively. The magnetic entropy of an $S = {}^1/_2$ spin system is expected to be $R\ln 2 = 5.76$ J K^{-1} mol^{-1}, where R is the gas constant. The present experimental magnetic entropy is very close to this expected value. This fact shows that the polycrystalline BABI sample is composed of pure and stable radicals with $S = {}^1/_2$ electron spins sites.

D. Magnetic Properties. The single-crystal X-ray crystallography[15] of BABI showed that bilayers made up of two sheets parallel to the *ab* plane are formed, whereas the magnetic susceptibility measurement[15] revealed that BABI's magnetism can be well expressed by the $S = {}^1/_2$ square-planar two-dimensional Heisenberg model with $J/k_B = -1.60$ K. At first, we tried to fit various one- and two-dimensional models to the magnetic heat capacity by use of a high-temperature series expansion, where extrapolation using Padé approximants was applied. Among them, the square-planar two-dimensional antiferromagnetic Heisenberg model[19] with $J/k_B = -1.6$ K showed satisfactory agreement with the ΔC_p values in the 4−10 K range where the magnetic phase transition does not seriously affect the curve shape. The resultant theoretical value is shown by a

TABLE 1: Molar Heat Capacities of BABI Crystal (M = 204.25 g mol^{-1})[a]

series 1						series 2		series 3									
T/K	C_p/ J K^{-1} mol^{-1}	T/K	C_p/ J K^{-1} mol^{-1}	T/K	C_p/ J K^{-1} mol^{-1}	T/K	C_p/ J K^{-1} mol^{-1}	T/K	C_p/ J K^{-1} mol^{-1}	T/K	C_p/ J K^{-1} mol^{-1}	T/K	C_p/ J K^{-1} mol^{-1}	T/K	C_p/ J K^{-1} mol^{-1}	T/K	C_p/ J K^{-1} mol^{-1}
0.463	0.0671	1.323	1.732	5.125	1.576	0.186	0.00522	1.122	0.9879	2.254	4.531	4.284	1.941	9.092	2.391	20.60	15.12
0.527	0.1095	1.437	2.346	5.618	1.485	0.218	0.0108	1.217	1.303	2.420	4.354	4.518	1.808	9.892	2.954	22.14	17.24
0.594	0.1305	1.577	3.290	6.163	1.467	0.245	0.0152	1.296	1.621	2.592	4.071	4.767	1.713	11.01	3.724	23.68	19.06
0.665	0.1873	1.730	4.374	6.751	1.519	0.268	0.0177	1.378	2.045	2.782	3.697	5.039	1.618	12.18	4.682	25.20	21.03
0.746	0.2423	1.917	4.496	7.386	1.618	0.306	0.0251	1.467	2.606	2.986	3.261	5.324	1.545	13.16	5.843	26.74	22.50
0.826	0.3393	2.274	4.461	8.070	1.854	0.338	0.0337	1.577	3.325	3.193	3.000	5.735	1.507	14.17	7.412	28.28	25.13
0.909	0.4653	2.838	3.441	8.810	2.213	0.372	0.0431	1.706	4.425	3.436	2.686	6.292	1.485	15.18	8.409		
1.003	0.6123	3.478	2.631	9.610	2.697	0.400	0.0566	1.841	4.621	3.633	2.463	6.931	1.552	16.21	9.600		
1.094	0.8746	4.021	2.092			0.448	0.0753	1.979	4.655	3.843	2.235	7.607	1.690	17.24	10.72		
1.192	1.258	4.548	1.822			0.513	0.0982	2.115	4.689	4.059	2.101	8.320	1.976	18.28	11.92		

series 4				series 5				series 6				series 7					
T/K	C_p/ J K^{-1} mol^{-1}	T/K	C_p/ J K^{-1} mol^{-1}	T/K	C_p/ J K^{-1} mol^{-1}	T/K	C_p/ J K^{-1} mol^{-1}	T/K	C_p/ J K^{-1} mol^{-1}	T/K	C_p/ J K^{-1} mol^{-1}	T/K	C_p/ J K^{-1} mol^{-1}	T/K	C_p/ J K^{-1} mol^{-1}	T/K	C_p/ J K^{-1} mol^{-1}
0.960	0.5348	1.510	2.783	4.047	2.114	10.09	3.061	5.666	1.562	15.19	7.996	6.725	1.627	18.21	12.31	30.45	30.37
1.022	0.6867	1.588	3.491	4.460	1.824	11.08	3.725	6.716	1.592	16.13	9.497	8.080	2.165	19.34	13.73	31.86	32.00
1.080	0.8530	1.666	4.111	4.902	1.642	12.11	4.622	7.383	1.766	17.09	10.76	9.383	2.880	20.47	15.51	33.25	33.54
1.141	1.008	1.738	4.414	5.391	1.534	13.10	5.745	8.254	2.229	18.05	11.96	10.61	3.746	21.63	17.28	34.64	35.51
1.204	1.233	1.817	4.473	5.919	1.469	14.10	7.335	9.213	2.748	18.98	13.29	11.77	4.686	22.77	18.82	36.05	37.61
1.259	1.454	1.908	4.500	6.489	1.469	15.11	7.867	10.20	3.437	19.93	14.95	12.88	5.708	23.97	20.61	37.46	39.40
1.311	1.642	2.070	4.599	7.102	1.549	16.34	9.601	11.24	4.238			13.92	6.827	25.23	22.34	38.90	40.86
1.371	1.945	2.331	4.391	7.762	1.715	18.58	11.95	12.23	5.012			14.95	8.014	26.43	24.51	40.34	42.55
1.439	2.245	2.650	3.902	8.478	2.020	19.59	13.42	13.21	6.029			15.99	9.177	27.70	26.31		
				9.252	2.478			14.20	7.124			17.09	10.77	29.07	28.36		

series 8																	
T/K	C_p/ J K^{-1} mol^{-1}	T/K	C_p/ J K^{-1} mol^{-1}	T/K	C_p/ J K^{-1} mol^{-1}	T/K	C_p/ J K^{-1} mol^{-1}	T/K	C_p/ J K^{-1} mol^{-1}	T/K	C_p/ J K^{-1} mol^{-1}	T/K	C_p/ J K^{-1} mol^{-1}	T/K	C_p/ J K^{-1} mol^{-1}	T/K	C_p/ J K^{-1} mol^{-1}
34.43	34.76	53.56	58.45	78.94	84.75	106.87	110.0	130.98	132.0	157.71	154.7	194.04	186.6	230.28	219.3	266.32	250.5
35.80	36.01	55.48	60.65	80.92	86.77	108.87	112.9	133.00	133.7	160.73	157.2	197.07	189.7	233.28	222.2	269.32	252.8
37.19	37.68	57.40	63.01	82.90	88.69	110.87	114.4	135.01	135.4	163.76	159.7	200.10	192.3	236.28	224.6	272.33	255.2
38.58	39.54	59.33	65.01	84.89	90.35	112.88	116.5	137.03	137.1	166.78	162.1	203.14	195.2	239.29	227.1	275.33	258.2
39.97	41.63	61.27	67.06	86.88	92.38	114.89	117.7	139.05	138.8	169.81	164.8	206.17	198.4	242.29	229.8	278.33	261.0
41.38	43.90	63.22	68.83	88.87	94.33	116.89	119.9	141.06	140.6	172.84	167.4	209.20	201.1	245.30	232.5	281.33	263.6
42.80	45.07	65.17	71.24	90.87	96.32	118.90	121.6	143.08	142.4	175.87	170.0	212.23	203.7	248.30	234.2	284.33	266.7
44.22	46.87	67.12	72.84	92.86	98.23	120.91	123.2	145.10	144.0	178.89	172.4	215.25	206.3	251.30	237.2	287.33	268.9
45.64	48.98	69.08	74.78	94.86	100.2	122.92	125.0	147.12	145.8	181.92	175.0	218.26	209.0	254.30	240.1	290.33	273.0
47.08	50.77	71.05	76.95	96.86	102.0	124.94	126.7	149.14	147.6	184.95	177.8	221.26	211.6	257.31	242.6	293.32	275.1
48.52	52.43	73.01	78.63	100.86	105.8	126.95	128.5	151.66	149.8	187.98	180.6	224.27	214.4	260.31	245.1	296.32	278.3
49.96	54.13	74.99	80.84	102.86	107.5	128.97	130.2	154.69	152.3	191.01	183.3	227.27	216.6	263.31	248.1	299.32	281.2
51.64	56.33	76.96	82.46	104.86	109.2												

[a] Data in series 1−5 and series 6−8 were collected by use of different adiabatic calorimeters.

dashed curve A in Figure 3b. This exchange interaction parameter agrees excellently well with the value obtained in the magnetic study.[15]

However, the BABI crystal lattice is actually characterized by the bilayer structure described above. A schematic drawing of the bilayer structure is shown in Figure 4. We therefore tried to fit the magnetic heat capacity by the high-temperature series expansion of an $S = {}^1/_2$ bilayer two-dimensional antiferromagnetic Heisenberg model with different intralayer and interlayer exchange interaction parameters,[20] also using Padé approximants. As the result, we obtained better fitting of the theoretical curve to the ΔC_p values in the 4−10 K temperature range when the intralayer interaction $J_1/k_B = -1.2$ K and the interlayer interaction $J_2/k_B = -1.9$ K. This theoretical curve is drawn by a solid curve B in Figure 3b.

According to the calculation of the radical−radical close contact exchange interactions for five BABI radical pairs by using the AMI−CI semiempirical molecular orbital method by Ferrer et al.,[15] the negative exchange interaction between the nitroxide groups through the *c*-axis inversion center is much larger than the positive ones for other four pairs. This situation enables us to regard the magnetic system of BABI crystal as a spin system in which two adjacent spins are strongly coupled with an antiferromagnetic exchange interaction, just like a dimer formation. Therefore, we fitted the following dimer (singlet−triplet) model[21] to the magnetic heat capacity in the 4−10 K region,

$$C_{\mathrm{dim}} = \frac{6RJ_{\mathrm{d}}^{\,2}\mathrm{e}^{2J_{\mathrm{d}}/k_{\mathrm{B}}T}}{k_{\mathrm{B}}^{\,2}T^2(1+3\mathrm{e}^{2J_{\mathrm{d}}/k_{\mathrm{B}}T})^2} \qquad (3)$$

The best fit was obtained when the intradimer exchange interaction $J_{\mathrm{d}}/k_{\mathrm{B}} = -2.8$ K, and the resultant curve is indicated by a dotted curve C in Figure 3b.

To examine the validity of the bilayer and dimer models in the magnetic behavior, we fitted the magnetic susceptibility data[15] in the 4−10 K range by the bilayer[20] and dimer[22] models together with the square-planar model,[19] where the Landé g

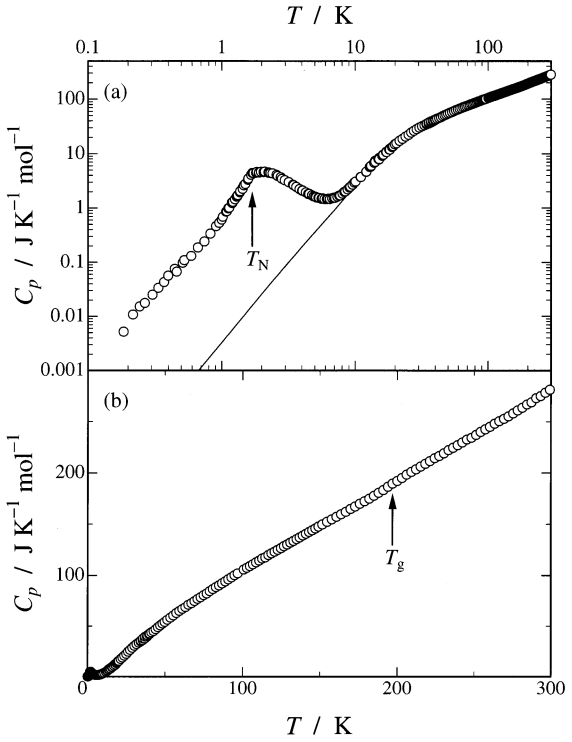

Figure 2. Molar heat capacity of BABI crystal on (a) logarithmic and (b) normal scales. Solid curve represents the lattice heat capacity. T_N shows the Néel temperature, and T_g a glassy transition temperature described in the text.

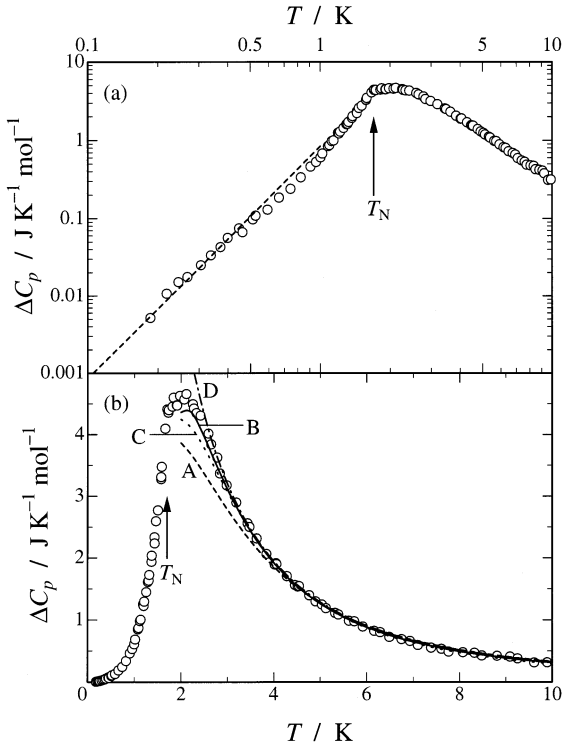

Figure 3. Magnetic heat capacity of BABI crystal on (a) logarithmic and (b) normal scales. Broken line drawn in plot (a) shows the heat capacity obtained from the spin wave theory for three-dimensional antiferromagnets. In plot (b), curves A and B indicate the heat capacities calculated on the basis of the high-temperature series expansion for the $S = {}^1/_2$ square-planar two-dimensional Heisenberg model with $J/k_B = -1.6$ K, and for the bilayer model with the intralayer interaction $J_1/k_B = -1.2$ K and the interlayer interaction $J_2/k_B = -1.9$ K, respectively. Curve C shows the heat capacity calculated by the dimer model with $J_d/k_B = -2.8$ K. Curve D represents the heat capacity calculated by the bilayer model with $J_1/k_B = -1.4$ K and $J_2/k_B = -1.3$ K derived from the magnetic data.

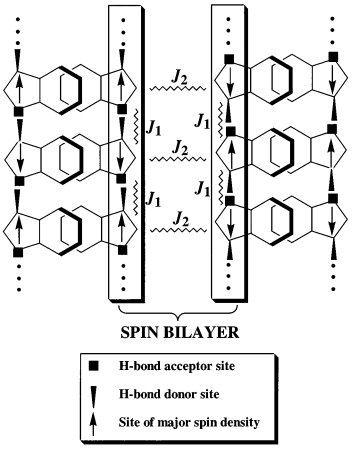

Figure 4. Schematic drawing of bilayer structure for BABI crystal.

factor was fixed to 2. As shown in Figure 5, good fitting results were obtained for the square-planar ($J/k_B = -1.6$ K) and bilayer ($J_1/k_B = -1.4$ K, $J_2/k_B = -1.3$ K) models, while very poor agreement was obtained for the dimer model ($J_d/k_B = -3.8$ K). Furthermore, we tried to compare the dimer model with a different value $J_d/k_B = -2.4$ K estimated from the relation $2J_d/k_B = -1.604T_{max}$, where T_{max} (= 3.01 K) corresponds to the temperature at which the magnetic susceptibility shows a maximum. However, the agreement was not improved (see Figure 5). Slight disagreement of the fitting parameters of the bilayer models between the calorimetric and magnetic data may be due to the experimental errors involved in both experiments. As shown in Figure 3b, the theoretical heat capacity calculated for the bilayer model by using the best-fit parameters ($J_1/k_B = -1.4$ K, $J_2/k_B = -1.3$ K) obtained for the magnetic susceptibility data also agree well with the experimental magnetic heat capacity. Similarly, the theoretical magnetic susceptibility calculated for the bilayer model by using the best-fit parameters ($J_1/k_B = -1.2$ K, $J_2/k_B = -1.9$ K) obtained for the heat capacity data (see Figure 5) shows fairly good agreement with the experimental magnetic susceptibility data. It should be remarked here that these two models should not be regarded as quite different origins: the bilayer model consists of two square-planar sheets between which magnetic interaction exists. In fact, the best-fit interaction parameter $J/k_B = -1.6$ K determined for the calorimetric and magnetic data is very close to the intralayer interaction parameters J_1/k_B determined by the best-fit to the heat capacity data (−1.2 K) and to the magnetic susceptibility (−1.4 K). Therefore, we can safely conclude that the spins in BABI crystal are arranged two-dimensionally in a square-planar way with antiferromagnetic interaction. As evidenced by the existence of a magnetic ordering phase transition, magnetic interaction actually exists between the square-planar sheets.

Magnetic heat capacities at very low temperatures are generally well approximated by the spin wave theory. The heat capacity due to the spin wave (magnon) excitation C_{SW} is expressed by the following equation[23]

$$C_{sw} \propto T^{d/n} \tag{4}$$

where d denotes the dimensionality of the magnetic lattice and n is defined as the exponent in the dispersion relation: $n = 1$ for antiferromagnets and $n = 2$ for ferromagnets. Analysis in terms of the spin wave theory approximated by eq 4 is often used for determination of the dimensionality of magnetic

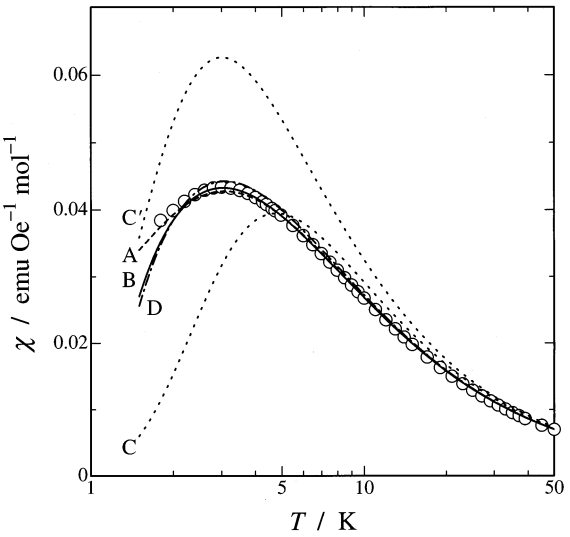

Figure 5. Magnetic susceptibility of BABI crystal. Curves A and B indicate the magnetic susceptibilities calculated on the basis of the high-temperature series expansion for the $S = {}^1/_2$ square planar two-dimensional Heisenberg model with $J/k_B = -1.6$ K and the bilayer model with the intralayer interaction $J_1/k_B = -1.4$ K and the interlayer interaction $J_2/k_B = -1.3$ K, respectively. Curves C and C′ show the magnetic susceptibilities calculated by the dimer models with $J_d/k_B = -3.8$ K and -2.4 K, respectively. Curve D represents the magnetic susceptibility calculated by the bilayer model using the exchange parameters $J_1/k_B = -1.2$ K and $J_2/k_B = -1.9$ K derived from the calorimetric data.

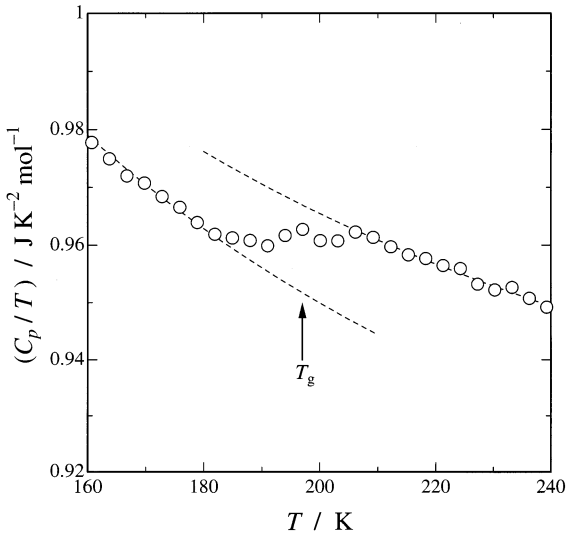

Figure 6. Molar heat capacity of BABI crystal divided by temperature in the vicinity of the glass transition.

ordering and the exchange interactions between spins. We fitted the following expression to the magnetic heat capacity below 0.53 K:

$$\Delta C_p = aT^{\alpha} \tag{5}$$

and obtained $\alpha = 2.74$. Since this value is close to ${}^d/_n = {}^3/_1$, we may conclude that the spins in BABI crystal order in a three-dimensional antiferromagnetic state below $T_N = 1.7$ K. This finding is quite important, since the bilayer model used to describe the magnetic behavior for $T > 1.7$ K would not yield magnetic ordering by itself. Such ordering arises due either to a small magnetic anisotropy or to extended interlayer interactions. Since dimensionality exponent $\alpha > 2$ in eq 5, the second mechanism is operant, i.e., the mechanism due to extended interlayer interactions (the so-called "dimensional crossover") is responsible for triggering three-dimensional magnetic ordering at lowest temperatures. Apparently, small additional interactions become important at very low temperatures, beyond those that are well-modeled by the bilayer model above the Néel temperature. These are likely due to close contacts between sites that possess small spin density populations, of which there are multiple candidates in the BABI crystal structure.[15] To model the low-temperature three-dimensional antiferromagnetic behavior, we again fitted eq 5 using a fixed value of $\alpha = 3$ to the magnetic heat capacity over the 4−10 K temperature region to obtain a value of $\alpha = 0.846$ J K^{-4} mol^{-1}. The spin wave heat capacity curve thus estimated is indicated by the broken line in Figure 3a.

E. Glass Transition. We observed a small thermal anomaly at around 200 K in the present BABI crystal as shown in Figure 2b. Although the change in temperature drift associated with enthalpy relaxation was not found, we may regard this anomaly as a glass transition from its shape. To confirm that this anomaly is due to glass transition, we plotted C_p/T versus T in Figure 6. Since the change from exothermic temperature drift to endothermic one usually encountered in ordinary glass transitions[24] was not found, the glass transition temperature was estimated as an inflection point of the heat capacity to be $T_g = 197$ K. In the variable temperature Fourier transform infrared (FT-IR) spectrometry,[15] the C−H and hydrogen-bonded N−H stretching bands were narrowing as temperature was decreased because of the hydrogen-bonding order in the crystal lattice and the slowing down of dynamical motion of the *tert*-butyl group on the nitroxide. There is a substantial narrowing of the envelope of FT-IR absorbances in the 3100−2800 cm^{-1} region as the temperature is decreased below 201 K. While this behavior is not definitive, it is consistent with the observed proposed process contributing to the glass transition. Furthermore, in the X-ray crystallography,[15] the equivalent displacement parameters of C and H atoms of methyl moieties in the *tert*-butyl group were quite large. From these experimental results, it is very likely that the observed glass transition might be due to freezing of the dynamical motion of the *tert*-butyl group on the nitroxide and/or of ordering of the hydrogen bonding in the crystal lattice. The lack of significant temperature drift change due to the enthalpy relaxation is perhaps caused by small enthalpy relaxation in the present glassy crystal.

4. Conclusions

We have performed heat capacity measurements of a new organic free radical, 2-*tert*-butylaminoxylbenzimidazole (BABI), which is stabilized through hydrogen bonding, in the temperature range between 0.2 and 299 K by adiabatic calorimetry. BABI crystal underwent a heat capacity cusp due to an antiferromagnetic phase transition at $T_N = 1.7$ K, above which it gave rise to a broad heat capacity anomaly centered around 2 K caused by the short-range order characteristic of low-dimensional magnetic systems. The enthalpy and entropy acquisitions due to the antiferromagnetic order amounted to 17.4 and 5.34 J K^{-1} mol^{-1}, respectively. The experimental entropy gain agrees well with the expected value for the magnetic ordering of $S = {}^1/_2$ spin systems, $R \ln 2 = 5.76$ J K^{-1} mol^{-1}. The heat capacity hump around 2 K was reproduced well by the $S = {}^1/_2$ two-dimensional antiferromagnetic bilayer Heisenberg model with the intralayer interaction $J_1/k_B = -1.2$ K and the interlayer interaction $J_2/k_B = -1.9$ K. The spin wave analysis of the magnetic heat capacity at very low temperatures shows that BABI exhibits extended magnetic ordering, and is a three-

dimensional antiferromagnet below T_N. Very recently, three analogous benzimidazole-based *tert*-butylnitroxide radicals have been synthesized and investigated magnetically.[25] Calorimetric study on these radicals and comparison with the present results are planned to elucidate further the mechanism of the magnetic ordering of BABI.

Acknowledgment. This study was partially supported by a grant-in-aid for scientific research on the priority areas of "Metal-Assembled Complexes" (Area No. 401/12023229) from the Ministry of Education, Culture, Sports, Science, and Technology, Japan. Support was also provided by the National Science Foundation (CHE 9809548), the Comision Interministerial de Ciencia y Tecnologia (MAT2000-1388-C03-03), and the Fullbright España commission.

References and Notes

(1) (a) Chouteau, G.; Veyret-Jeandey, Cl. *J. Phys. (Paris)* **1981**, *42*, 1441. (b) Benoit, A.; Flouquet, J.; Gillon, B.; Schweitzer, J. *J. Magn. Magn. Mater.* **1983**, *31*−*34*, 1155.

(2) (a) Kinoshita, M.; Turek, P.; Tamura, M.; Nozawa, K.; Shiomi, D.; Nakazawa, Y.; Ishikawa, M.; Takahashi, M.; Awaga, K.; Inabe, T.; Maruyama, Y. *Chem. Lett.* **1991**, 1225. (b) Takahashi, M.; Turek, P.; Nakazawa, Y.; Tamura, M.; Nozawa, K.; Shiomi, D.; Ishikawa, M.; Kinoshita, M. *Phys. Rev. Lett.* **1991**, *67*, 746. (c) Tamura, M.; Nakazawa, Y.; Shiomi, D.; Nozawa, K.; Hosokoshi, Y.; Ishikawa, M.; Takahashi, M.; Kinoshita, M. *Chem. Phys. Lett.* **1991**, *186*, 401. (d) Nakazawa, Y.; Tamura, M.; Shirakawa, N.; Shiomi, D.; Takahashi, M.; Kinoshita, M.; Ishikawa, M. *Phys. Rev. B* **1992**, *46*, 8906.

(3) (a) Allemand, P.-M.; Khemani, K. C.; Koch, A.; Wudl, F.; Holczer, K.; Donovan, S.; Grüner, G.; Thompson, J. D. *Science* **1991**, *253*, 301. (b) Tanaka, K.; Zakhidov, A. A.; Yoshizawa, K.; Okahara, K.; Yamabe, T.; Yakushi, K. *Phys. Rev. B* **1993**, *47*, 7554. (c) Mihailovic, D.; Arcon, D.; Venturini, P.; Blinc, R.; Omerzu, A.; Cevc, P. *Science* **1995**, *268*, 400.

(4) (a) Sugimoto, H.; Aota, H.; Harada, A.; Morishima, Y.; Kamachi, M.; Mori, W.; Kishita, M.; Ohmae, N.; Nakano, M.; Sorai, M. *Chem. Lett.* **1991**, 2095. (b) Kamachi, M.; Sugimoto, H.; Kajiwara, A.; Harada, A.; Morishima, Y.; Mori, W.; Ohmae, N.; Nakano, M.; Sorai, M.; Kobayashi, T.; Amaya, K. *Mol. Cryst. Liq. Cryst.* **1993**, *232*, 53. (c) Kobayashi, T.; Takiguchi, M.; Amaya, K.; Sugimoto, H.; Kajiwara, A.; Harada, A.; Kamachi, M. *J. Phys. Soc. Jpn.* **1993**, *62*, 3239. (d) Kajiwara, A.; Sugimoto, H.; Kamachi, M. *Bull. Chem. Soc. Jpn.* **1994**, *67*, 2373. (e) Ohmae, N.; Kajiwara, A.; Miyazaki, Y.; Kamachi, M.; Sorai, M. *Thermochim. Acta* **1995**, *267*, 435. (f) Kajiwara, A.; Mori, W.; Sorai, M.; Yamaguchi, K.; Kamachi, M. *Mol. Cryst. Liq. Cryst.* **1995**, *272*, 67. (g) Kobayashi, T. C.; Takiguchi, M.; Hong, C. U.; Amaya, K.; Kajiwara, A.; Harada, A.; Kamachi, M. *J. Magn. Magn. Mater.* **1995**, *140*−*144*, 1447.

(5) (a) Chiarelli, R.; Rassat, A.; Pey, P. *J. Chem. Soc., Chem. Commun.* **1992**, 1081. (b) Chiarelli, R.; Novak, M. A.; Rassat, A.; Tholence, J. L. *Nature* **1993**, *363*, 147.

(6) (a) Mukai, K.; Nedachi, K.; Jamali, J. B.; Achiwa, N. *Chem. Phys. Lett.* **1993**, *214*, 559. (b) Mukai, K.; Konishi, K.; Nedachi, K.; Takeda, K. *J. Magn. Magn. Mater.* **1995**, *140*−*144*, 1449. (c) Mukai, K.; Kawasaki, K.; Jamali, J. B.; Achiwa, N. *Chem. Phys. Lett.* **1995**, *241*, 618. (d) Mukai, K.; Konishi, K.; Nedachi, K.; Takeda, K. *J. Phys. Chem.* **1996**, *100*, 9658. (e) Mukai, K.; Wada, N.; Jamali, J. B.; Achiwa, N.; Narumi, Y.; Kindo, K.; Kobayashi, T.; Amaya, K. *Chem. Phys. Lett.* **1996**, *257*, 538. (f) Mukai, K.; Nuwa, M.; Morishita, T.; Muramatsu, T.; Kobayashi, T. C.; Amaya, K. *Chem. Phys. Lett.* **1997**, *272*, 501. (g) Mino, M.; Takeda, K.; Mukai, K.; Azuma, N.; Gleiter, M. R.; Krieger, C.; Neugebauer, F. A. *J. Phys. Chem. B* **1997**, *101*, 9517. (h) Mukai, K.; Wada, N.; Jamali, J. B.; Achiwa, N.; Narumi, Y.; Kindo, K.; Kobayashi, T.; Amaya, K. *Mol. Cryst. Liq. Cryst.* **1997**, *305*, 499. (i) Mukai, K.; Nuwa, M.; Suzuki, K.; Nagaosa, S.; Achiwa, N.; Jamali, J. B. *J. Phys. Chem. B* **1998**, *102*, 782.

(7) (a) Kremer, R. K.; Kanellakopulos, B.; Bele, H.; Brunner, H.; Neugebauer, F. A. *Chem. Phys. Lett.* **1994**, *230*, 255. (b) Tomiyoshi, S.; Yano, T.; Azuma, N.; Shoga, M.; Yamada, K.; Yamauchi, *J. Phys. Rev. B* **1994**, *49*, 16031.

(8) (a) Sugawara, T.; Matsushita, M. M.; Izuoka, A.; Wada, N.; Takeda, N.; Ishikawa, M. *J. Chem. Soc., Chem. Commun.* **1994**, 1723. (b) Sugawara, T.; Izuoka, A. *Mol. Cryst. Liq. Cryst.* **1997**, *305*, 41.

(9) (a) Nogami, T.; Tomioka, K.; Ishida, T.; Yoshikawa, H.; Yasui, M.; Iwasaki, F.; Iwamura, H.; Takeda, N.; Ishikawa, M. *Chem. Lett.* **1994**, 29. (b) Ishida, T.; Tsuboi, H.; Nogami, T.; Yoshikawa, H.; Yasui, M.; Iwasaki, F.; Iwamura, H.; Takeda, N.; Ishikawa, M. *Chem. Lett.* **1994**, 919. (c) Nogami, T.; Ishida, T.; Yoshikawa, H.; Yasui, M.; Iwasaki, F.; Iwamura, H.; Takeda, N.; Ishikawa, M. *Synth. Met.* **1995**, *71*, 1813. (d) Nogami, T.; Ishida, T.; Tsuboi, H.; Yoshikawa, H.; Yamamoto, H.; Yasui, M.; Iwasaki, F.; Iwamura, H.; Takeda, N.; Ishikawa, M. *Chem. Lett.* **1995**, 635. (e) Nogami, T.; Ishida, T.; Yasui, M.; Iwasaki, F.; Iwamura, H.; Takeda, N.; Ishikawa, M. *Mol. Cryst. Liq. Cryst.* **1996**, *279*, 97. (f) Togashi, K.; Imachi, R.; Tomioka, K.; Tsuboi, H.; Ishida, T.; Nogami, T.; Takeda, N.; Ishikawa, M. *Bull. Chem. Soc. Jpn.* **1996**, *69*, 2821. (g) Nogami, T.; Imachi, R.; Ishida, T.; Takeda, N.; Ishikawa, M. *Mol. Cryst. Liq. Cryst.* **1997**, *305*, 211. (h) Miyazaki, Y.; Matsumoto, T.; Ishida, T.; Nogami, T.; Sorai, M. *Bull. Chem. Soc. Jpn.* **2000**, *73*, 67.

(10) (a) Cirujeda, J.; Mas, M.; Molins, E.; Lanfranc de Panthou, F.; Laugier, J.; Park, J. G.; Paulsen, C.; Rey, P.; Rovira, C.; Veciana, J. *J. Chem. Soc., Chem. Commun.* **1995**, 709. (b) Cirujeda, J.; Ochando, L. E.; Amigó, J. M.; Rovira, C.; Rius, J.; Veciana, J. *Angew. Chem., Int. Ed. Engl.* **1995**, *34*, 55. (c) Cirujeda, J.; Hernàndez-Gasió, E.; Lanfranc de Panthou, F.; Laugier, J.; Mas, M.; Molins, E.; Rovira, C.; Novoa, J. J.; Rey, P.; Veciana, J. *Mol. Cryst. Liq. Cryst.* **1995**, *271*, 1. (d) Cirujeda, J.; Hernàndez-Gasió, E.; Rovira, C.; Stanger, J.-L.; Turek, P.; Veciana, J. *J. Mater. Chem.* **1995**, *5*, 243. (e) Novoa, J. J.; Deumal, M.; Kinoshita, M.; Hosokoshi, Y.; Veciana, J.; Cirujeda, J. *Mol. Cryst. Liq. Cryst.* **1997**, *305*, 129.

(11) (a) Caneschi, A.; Ferraro, F.; Gatteschi, D.; Le Lirzin, A.; Rentschler, E. *Inorg. Chim. Acta* **1995**, *235*, 159. (b) Caneschi, A.; Ferraro, F.; Gatteschi, D.; Lirzin, A.; Novak, M. A.; Rentschler, E.; Sessoli, R. *Adv. Mater.* **1995**, *7*, 476.

(12) Sugimoto, T.; Tsuji, M.; Suga, T.; Hosoito, N.; Ishikawa, M.; Takeda, N. *Mol. Cryst. Liq. Cryst.* **1995**, *272*, 183.

(13) (a) Banister, A. J.; Bricklebank, N.; Clegg, W.; Elsegood, M. R. J.; Gregory, C. I.; Lavender, I.; Rawson, J. M.; Tanner, B. K. *J. Chem. Soc., Chem. Commun.* **1995**, 679. (b) Banister, A. J.; Bricklebank, N.; Lavender, I.; Rawson, J. M.; Gregory, C. I.; Tanner, B. K.; Clegg, W.; Elsegood, M. R. J.; Palacio, F. *Angew. Chem., Int. Ed. Engl.* **1996**, *35*, 2533. (c) Palacio, F.; Castro, M.; Antorrena, G.; Burriel, R.; Ritter, C.; Bricklebank, N.; Rawson, J.; Smith, J. N. B. *Mol. Cryst. Liq. Cryst.* **1997**, *306*, 293. (d) Palacio, F.; Antorrena, G.; Castro, M.; Burriel, R.; Rawson, J.; Smith, J. N. B.; Bricklebank, N.; Novoa, J.; Ritter, C. *Phys. Rev. Lett.* **1997**, *79*, 2336.

(14) (a) Yoshioka, N.; Irisawa, M.; Mochizuki, Y.; Kato, T.; Inoue, H.; Ohba, S. *Chem. Lett.* **1997**, 251. (b) Yoshioka, N.; Irisawa, M.; Mochizuki, Y.; Aoki, T.; Inoue, H. *Mol. Cryst. Liq. Cryst.* **1997**, *306*, 403.

(15) Ferrer, J. R.; Lahti, P. M.; George, C.; Antorrena, G.; Palacio, F. *Chem. Mater.* **1999**, *11*, 2205.

(16) Murakawa, S.; Wakamatsu, T.; Nakano, M.; Sorai, M.; Suga, H. *J. Chem. Thermodyn.* **1987**, *19*, 1275.

(17) Kume, Y.; Miyazaki, Y.; Matsuo, T.; Suga, H. *J. Phys. Chem. Solids* **1992**, *53*, 1297.

(18) J. Blöte, H. M. *Phys. B* **1975**, *79*, 427.

(19) Baker, G. A., Jr.; Gilbert, H. E.; Eve, J.; Rushbrooke, G. S. *Phys. Lett.* **1967**, *25A*, 207.

(20) Weilong, Z. *Phys. Rev. B* **1997**, *55*, 12267.

(21) Kambe, K. *J. Phys. Soc. Jpn.* **1950**, *5*, 48.

(22) Bleaney, B.; Bowers, K. D. *Proc. R. Soc. London A* **1952**, *214*, 451.

(23) de Jongh L. J.; Miedema, A. R. *Adv. Phys.* **1974**, *23*, 1.

(24) Suga, H.; Seki, S. *J. Non-Cryst. Solids* **1974**, *16*, 171.

(25) Lahti, P. M.; Ferrer, J. R.; George, C.; Oliete, P.; Julier, M.; Palacio, F. *Polyhedron* **2001**, *20*, 1465.